HAL open science

# Osteochondral repair combining therapeutics implant with mesenchymal stem cells spheroids

Henri Favreau, Luc Pijnenburg, Joseph Seitlinger, Florence Fioretti, Laetitia Keller, Dominique Scipioni, Hans Adriaensen, Sabine Kuchler-Bopp, Matthieu Ehlinger, Didier Mainard, et al.

## To cite this version:

Henri Favreau, Luc Pijnenburg, Joseph Seitlinger, Florence Fioretti, Laetitia Keller, et al.. Osteochondral repair combining therapeutics implant with mesenchymal stem cells spheroids. Nanomedicine: Nanotechnology, Biology and Medicine, 2020, 29, pp.102253. 10.1016/j.nano.2020.102253 . hal-02924928

**HAL Id: hal-02924928**

**https://hal.inrae.fr/hal-02924928v1**

Submitted on 22 Aug 2022

**HAL** is a multi-disciplinary open access archive for the deposit and dissemination of scientific research documents, whether they are published or not. The documents may come from teaching and research institutions in France or abroad, or from public or private research centers.

L'archive ouverte pluridisciplinaire **HAL**, est destinée au dépôt et à la diffusion de documents scientifiques de niveau recherche, publiés ou non, émanant des établissements d'enseignement et de recherche français ou étrangers, des laboratoires publics ou privés.

Distributed under a Creative Commons Attribution - NonCommercial 4.0 International License

Version of Record: https://www.sciencedirect.com/science/article/pii/S1549963420301076
Manuscript_35f6a614a711d0e2d571f54bce3e26e4

# Osteochondral Repair Combining Therapeutics Implant with Mesenchymal Stem Cells Spheroids

Henri Favreau, Dr. [a,c,g], Luc Pijnenburg, Dr. [a,c,g], Joseph Seitlinger, Dr. [a,c,g], Florence Fioretti Dr. [a,b,g], Laetitia Keller Dr. [a,b,g], Dominique Scipioni Dr. [d], Hans Adriaensen Dr. [e], Sabine Kuchler-Bopp Dr. [a], Matthieu Ehlinger Dr. [a,c], Didier Mainard Dr. [a,f], Phillippe Rosset Dr. [e], Guoqiang Hua Dr. [a,b], Luca Gentile Dr. [a,b] and Nadia Benkirane-Jessel Dr. [a,b,*]

[a]INSERM (French Institute of Health and Medical Research), UMR 1260, Regenerative Nanomedicine (RNM), FMTS, 67000 Strasbourg, France.

[b]Université de Strasbourg, Faculté de Chirurgie Dentaire, 67000 Strasbourg, France.

[c]Hôpitaux universitaires de Strasbourg (HUS), Hôpital de Hautepierre, Service de rhumatologie, Service de chirurgie thoracique and Service de chirurgie orthopédique et de traumatologie, Université de Strasbourg, 67000 Strasbourg, France.

[d]Hôpital Erasme - Cliniques universitaires de Bruxelles, Université libre de Bruxelles (ULB), CHIREC - Hôpital Delta, 1070 Bruxelles, Belgique.

[e]CHRU de Tours, Service de Chirurgie Orthopédique 2, Faculté de Médecine de Tours, and INRA de tours, Université François Rabelais, 37000 Tours, France.

[f]Hôpital central Nancy, Service d'Orthopédie, 54000 Nancy, France.

[g]These authors contributed equally to this work.

**Conflicts of Interest:** The authors declare no competing financial interests.

**Funding:** This work was supported by SATT CONECTUS Alsace "Projet Maturation".

*Corresponding author at: INSERM UMR 1260, Regenerative Nanomedicine (RNM), 67000 Strasbourg, France.

*E-mail address: nadia.jessel@inserm.fr (N. B.-J.)*

Abstract: 150 words

Complete manuscript word count (body text and figure legends): 4968 words

Number of references: 60

Number of figures: 5



© 2020 published by Elsevier. This manuscript is made available under the CC BY NC user license
https://creativecommons.org/licenses/by-nc/4.0/

**Abstract**

Functional articular cartilage regeneration remains challenging, and it is essential to restore focal osteochondral defects and prevent secondary osteoarthritis. Combining autologous stem cells with therapeutic medical device, we developed a bi-compartmented implant that could promote both articular cartilage and subchondral bone regeneration. The first compartment based on therapeutic collagen associated with bone morphogenetic protein 2, provides structural support and promotes subchondral bone regeneration. The second compartment contains bone marrow-derived mesenchymal stem cell spheroids to support the regeneration of the articular cartilage. Six-month post-implantation, the regenerated articular cartilage surface was 3 times larger than that of untreated animals, and the regeneration of the osteochondral tissue occurred during the formation of hyaline-like cartilage. Our results demonstrate the positive impact of this combined advanced therapy medicinal product, meeting the needs of promising osteochondral regeneration in critical size articular defects in a large animal model combining not only therapeutic implant but also stem cells.

*Keywords:* Bi-compartmented Nanoactive Therapeutics, Osteochondral Regeneration, Cartilage repair, Sheep, Mesenchymal stem cells

## Background

Articular cartilage restoration remains challenging due to the limited physiological repair potential of human osteochondral tissue, as noticed almost two hundred years ago by anatomist William Hunter[1]. Although current techniques (*e.g.*, bone graft, micro-fracture, mosaicplasty), have shown some promising results in the short term, they remain invasive, painful and may provoke adverse effects[2]. The stimulation of the bone marrow by micro-fracture allows complete filling of the osteochondral defect; however, the regenerated tissue is characterized by the presence of fibrocartilage[3], which does not prevent secondary osteoarthritis[4]. Matrix-assisted autologous chondrocyte transplantation (MACT), another technique that uses xenogeneic scaffolds (*e.g.*, Chondro-Gide®, CaReS®, Novocart® 3D) for cartilage repair[5,6], but also induces fibrocartilage formation and may cause new defects (due to the necessity of autologous chondrocyte sampling)[7]. Moreover, ≥ 60% of patients undergoing knee arthroscopy showed osteochondral defects[8]. Therefore, a plethora of new strategies have been developed in the last two decades, to offer potential alternatives to the current treatments. The development of third generation therapeutics that combine synthetic or natural materials with active biomolecules and living cells is aimed to stimulate specific cellular responses[9,10], achieving multiple tissue regeneration. In this context, by analogy with bone repair in fractured sites, functionalized scaffolds with collagen matrix soaked with bone morphogenetic protein 2 (BMP-2) produced by InductOs® implant (Medtronic) could be developed. However, the massive release of BMP-2 has severe consequences[11–15]. The patented nanocontainer technology developed in our team could efficiently reduce these adverse effects via cell contact dependent local releases of therapeutics such as growth factors at physiological levels[16,17]. Recently, bone marrow-derived mesenchymal stem cells (MSCs) as advanced therapy medicinal products (ATMPs), have been reported as a suitable alternative for bone and cartilage regeneration, owing to their immunomodulatory and self-renewal properties[18,19], and can be easily harvested in a patient through bone marrow aspiration. Most importantly, their potential to differentiate in chondrocytes, makes the harvesting of autologous chondrocytes obsolete, and therefore avoids impairment of the patients healthy cartilage tissue[20–22]. After harvesting, MSCs can be cultured as spheroids, which improves their ability to differentiate into chondrogenic and osteogenic lineages, as has been previously shown[23–27]. Since the subchondral bone plays a central role in the homeostasis of the cartilage, its regeneration is also fundamental to increase the long term-stability of the newly regenerated cartilage tissue in focal osteochondral defects (less than 5 $cm^2$). We have previously shown that the combination of a collagen membrane functionalized with BMP-2-containing nanocontainers (NCs) and MSC spheroids embedded in hydrogel promoted the formation of both cellular and extracellular matrix gradients, within the osteochondral unit[28–30]. Recently, we have reported that by combining a FDA-approved resorbable polymeric Poly-ε-caprolactone (PCL) nanofibrous bone wound dressing and bone marrow-derived mesenchymal stem cells could efficiently and safely treat osteochondral defects in a large animal model[31]. The objective of this work was to show that combining collagen bone wound dressing and MSC spheroids embedded in hydrogel, our bi-compartmented advanced therapy medicinal product (ATMP; see Figure 1) allows

the functional regeneration of the entire subchondral unit in a large animal model. The osteoarticular regeneration process was evaluated non-invasively by magnetic resonance imaging (MRI), X-ray micro-computed tomography (Micro-CT) and macroscopic assessment according to the International Cartilage Repair Society (ICRS) score.

In conclusion, we showed how our combined ATMPs bi-compartmented therapeutics (BCT) could stimulate the simultaneous regeneration of the two main tissues that form the articulation, the cartilage and the subchondral bone in a large animal model.

**Methods**

Animal experimental implantation procedure

A total of 4 healthy, skeletally mature sheep ("Ile de France"), aged between 2 and 3 years, were included in this study. The experiments were performed in accordance with the European directive 2010/63/EU for animal protection and welfare used for scientific purposes and approved by the local ethical committee for animal experimentation (CEEA VdL N°19, Tours, France, authorization N° 2015031015102515-424, Issued the 8 of October 2015) for five years. This study was designed based on the international ethical 3R principal: reduce, replace and refine.

For aspiration of 20-30 ml of bone marrow from the iliac crest in heparinized syringe, sheep were anaesthetized by intravenous injection of Xylazine (0.05 mg/kg) and Ketamine (5 mg/Kg). MSCs were then isolated from the total bone marrow through a culture process. One month after bone marrow aspiration, animals were anaesthetized by intravenous injection of Xylazine (0.05 mg/kg) and Ketamine (5 mg/Kg) and endotracheally intubated with 100% $O_2$ and 5% isoflurane to maintain anesthesia.

For surgery, sheep were placed in dorsal recumbency. In sterile conditions, the hind limb was flexed to a position at which the medial condyle could be palpated under the skin. A 15 cm medial parapatellar skin incision was performed. After blunt dissection of the subcutaneous tissues, the fascia overlying the vastus medialis muscle was incised just distal to the belly muscle with a small incision parallel to the muscle fibers and the vastus was retracted proximally. Blunt dissection was used to expose the periosteum down to the medial condyle of the femur. The joint capsule and periosteum were incised just proximal to the origin of the medial collateral ligament. Overlying soft tissues were removed from the bone only in the vicinity of the drill holes. A total of 12 osteochondral defects (7 mm diameter by 3 mm depth) were created using a 6-mm drill bit in 4 sheep (see Table S1). In the control group (n=6, in sheep N° 1 and 2, and n=2, no defect control), lesions were performed and left untreated. In our procedure with the combined ATMP (n=6, in sheep N° 3 and 4, and n=2, no defect control), the first step was to cover the subchondral bone lesion by the BMP-2 active collagen membrane, and the second step was to implement the hydrogel solution (alginate/hyaluronic acid) containing autologous MSCs spheroids, in order to macroscopically fill the defect. Jellification of the hydrogel was then performed by injection of $CaCl_2$. The knee joint was repositioned, the patellar tendon was sutured as well as the leg wound, which was sutured layer by layer. The animals received a single post-surgical

injection of morphine (10 mg/sheep) and were then free to move. After 6 months, euthanasia was performed using lethal dose of sodium pentobarbital by intravenous injection in the jugular vein.

Therapeutic implants preparation

For the formation of the BMP-2 active part of the implant, collagen Bio-Gide® (Geistlich Pharma France) membranes (30 x 40 mm and cut according to bone lesion size) were alternately dipped during 15 minutes in solutions of BMP-2 (rh-BMP-2, Inductos®, Medtronic, France, 200 ng/ml, in pH 5.5 MES buffer) and chitosan (Chitosan, Protasan UP CL 113, Novamatrix, Sandvika, Norway, 0.5 mg/ml in MES), with a step of MES buffer bath (40 mM of 4-Morpholino-ethane-sulfonic acid, and 150 mM sodium chloride, Sigma-Aldrich, pH=5.5) after each dip. To form nanoreservoirs of BMP-2, this cycle was repeated 12 times. The nanofunctionalized collagen membranes were then stored at 4°C in MES buffer until their implantation.

The hydrogel part of the implant was produced by dissolution of sodium alginate (12 mg/ml, Sigma-Aldrich) and hyaluronic acid (3 mg/ml, Lifecore Biomedical, Chaska, USA) in sodium chloride (9 mg/ml, Sigma-Aldrich). Autologous MSCs were sub-cultured in suspension using a multi-well culture plate (GravityPLUSTM 3D Culture, InSphero AG, Zurich, Switzerland) to form spheroids in proliferation culture medium. After 5 days, they were collected to be suspended in the alginate/hyaluronic acid solution, at a final concentration of $10^7$ cells/ml, and aspired in a syringe under sterile laminar flow to be transported at 37°C until surgical procedure. The hydrogel was applied onto the implanted nanoactive membrane, and then jellified using calcium chloride (102 mM, Sigma-Aldrich).

*Measurement of regenerated cartilage*

Before 3D volume rendering micro-CT acquisitions, two slides intersecting the center of the original defect were analyzed for average cartilage regeneration thickness. Area of regenerated cartilage covering bone was measured (Osirix program) for each slide, and the mean area calculated to estimate quantitatively the cartilage recovering degree of the defects (n=5 for non-treated defects; n=5 for treated defects). Values were expressed as mean ± SEM. Statistical analyses (t-student) were performed using BiostaTGV program. Differences were considered significant at $p < 0.05$.

*Histological analyses of repaired cartilage*

At 6 months post-implantation, 3 mm diameter biopsies were performed in the superficial phase of each implanted site. Biopsies were then embedded in optimum cutting temperature medium, 20 µm cryostat sections were performed and laid on gelatin coated glasses. For total glycosaminoglycans staining, a solution of 2% (*m/v*) Alcian Blue (Sigma-Aldrich) at pH 4.2 was added on samples during 2 hours at room temperature after rinsing with distilled water. For sulphated glycosaminoglycans staining, samples were soaked in distilled water and dipped alternately in a solution of Fast Green

(0.02% *m/v*), acetic acid (1% *m/v*), and Safranin-O (0.1% *m/v*). Slides were analyzed under a bright field microscope (Leica DM 4000B) after mounting with Histolaque LMR® (LaboModerne, France).

*Statistical analysis*

GraphPad Prism 5 was used for both the statistical analyses and the plotting of the data, with the except for the violin chart, done wire R (with packages ggplot2 and vioplot). The relative areas of the hyper-intense signal detected with MRI as well as the areas of cartilage regeneration detected with CT-scan were analyzed with two-tailed unpaired t-test.

## Results

*Stemness validation of sheep bone marrow MSCs*

The proper characterization of MSCs for clinical application is very important, as MSC features are both source tissue-related and age-dependent[32,33]. Therefore, we characterized the MSCs used in this study according to the recommendations of the International Society for Cellular Therapy (ISCT, 2006). In accordance to these recommendations, the expression profile of a set of clusters of differentiation (CD) markers was investigated via immunostaining combined to flow cytometry (Figure S1, *A*). Owing to the lack of commercially available antibodies for sheep, antibodies reactive to human cells were used to characterize the MSCs aspirated from sheep bone marrow. No signal was observed for CD34, CD73 and CD105 markers, which was attributed to the limited cross-reactivity between man and sheep species, as reported in other studies[34,35]. Only a minor proportion of the cell population was positive for CD90 (11,14±0.3%), haematopoietic CD45 (6±1.7%) and major histocompatibility complex (MHC) class II receptor HLA-DR (3.8±0,7%). On the contrary, the large majority of the cells were found positive to CD44 (92.1±1,2%) and CD166 (86.9±2%), suggesting a high purity of the MSC population.

After *in vitro* culture, sheep MSCs were able to generate colony-forming unit-fibroblast (CFU-F) (Figure S1, *B*), implying that the self-renewal ability of these cells was preserved. Besides the biochemical characterization and the ability to self-review, the one feature important to support the regeneration of missing/damaged tissues is the multipotency of the utilized MSCs. We investigated the ability of the bone marrow-derived sheep MSCs to differentiate in chondrocytes, osteocytes and adipocytes. After 28 days of differentiation in chondrogenic medium, cells were found positive for the presence of glycosaminoglycans (GAGs), characteristic of chondrocytes (Figure S1, *C*). After allowing the cells to proliferate over 3 days, MSCs were cultured under osteogenic conditions for 21 days. Mineralization via deposition of calcium was confirmed by Alizarin red staining (Figure S1, *D*). In parallel, the capability of the MSCs to differentiate in adipocytes was also tested. After three cycles of adipogenic induction for a total of 28 days, the presence of lipid-rich vacuoles was proved by Oil Red O staining (Figure S1, *E*). These experiments showed that sheep MSCs harvested from their bone marrow maintained their multipotency under our culture conditions and were therefore suitable to use for the regeneration of the osteochondral articulation.

As we previously showed, materials nano-functionalized with osteogenic factors, such as BMP-2 or BMP-7[16,17], support MSCs for bone regeneration[25,26]. In order to promote the restoration of a functional subchondral unit, we added MSC spheroids embedded in hydrogel to the nano-functionalized scaffold, to enhance chondrogenic differentiation[29,36].

*Non-invasive imaging of the treated articulations with Magnetic Resonance Imaging (MRI)*

The bi-compartmented therapeutics (BCT) was implanted via a one-step surgery, in osteochondral defects, that were drilled in the medial femoral condyles of sheep during the same procedure. Follow-up time was 6 months after the implantation procedure. No signs of synovitis, joint effusion or fracture were observed after the surgery, and all sheep survived the experimental period. In order to evaluate the level of tissue repair, the final result was based on the International Cartilage Repair Society (ICRS) score system, evaluating the macroscopic repair of the defect (filling degree, integration within the host tissues, and the general aspect of the newly formed cartilage), 6 months after surgery. In addition, a non-invasive evaluation of the regeneration of the articular cartilage was also carried on with MRI analysis. Treated sheep joints were imaged three times during the follow up: immediately after surgery ($t_0$), 3 months and 6 months after surgery (Figure 2, *A-I*). Edema-like hyper-intense T2 weighted signals that were not observed in wild-type condyles (Figure 2, *A*) were observed in the subchondral sites after surgery, which are consistent with the inflammation induced by the surgical procedure (red dashed lines in Figure 2, *D and G*), in agreement with previous observations[37]. With the healing process ongoing, hyper-intense T2 signal is usually replaced by a hypo-intense signal, owing to the replacement of the inflammatory tissue by fibrotic tissue[38]. Consequently, the intensity of the signal observed 3 months post-surgery (Figure 2, *B, E and H*) was generally higher than that recorded 6 months post-surgery (Figure 2, *C, F and I*). As pointed out by several authors, persistent edema-like hyper-intense signal is generally associated with poor articular regeneration[39,40]. Following autologous chondrocyte implantation (ACI) in clinical trials, authors concluded that delays in the switch from hyper-intense to hypo-intense MRI signals (generally occurring 1-2 years post-surgery), is associated with poor outcome [38]. Although our follow up period was too short to observe complete regression of the subchondral hyper-intense signals, a substantial decrease of the signal intensity between 3 months and 6 months after surgery was observed in 5 out of 6 condyles implanted with the BCT, and in 5 out of 6 untreated control condyles. However, the intensity of such a signal was significantly lower in BCT-implanted sheep compared to the untreated defect control group at both 3 (730.2 ± 102.2 pixel vs. 896.0 ± 104.0 pixel, respectively; $p = 0.0193$) and 6 months (379.5 ± 175.4 pixel vs. 607.5 ± 148.1 pixel, respectively; $p = 0.0352$) post-surgery (Figure 2, *J*). Since post-mortem analysis (ICRS scores for the evaluation of the osteochondral tissue regeneration and micro-CT scans for the assessment of the surface of new cartilage formed) confirmed the synergistic effect of the BCT to restore both bone and cartilage (see next paragraphs), we concluded that the signal intensity obtained with MRI is a useful marker for monitoring non-invasively the post-surgery healing process after clinical treatments, also in the short/medium term.

*Post-mortem assessment of the articulations indicates the regeneration potential of the BCT*

Six months post-surgery, sheep were sacrificed, and BCT-implanted as well as untreated defect control condyles were explanted for the macroscopic evaluation of the regeneration of the osteochondral unit. The macroscopic evaluation of the explanted condyles according to the ICRS scoring system showed that condyles transplanted with the BCT have in general a better appearance (Figure 3, *A-B*) and that a degree of defect repair between 75% and 100% was achieved in 3 out of 6 condyles transplanted with the BCT and only in 1 out of 6 control condyles (untreated defects) (Figure 3, *A-B*). Also, a good integration of the graft (indicated by a demarcating border thinner than 1 mm) was confirmed in 3 out of 6 implanted condyles (Figure 3, *B*). Fibrillated-to-smooth surface appearance was observed in the other 3 BCT-transplanted specimens.

Micro-CT images obtained on the explanted condyles revealed in all samples an irregular surface of the mineralized part of the implant (Figure 3, *C*). However, the 2D projections revealed signs of bone healing and remodeling, with bone condensation close to the articular surface (Figure 3, *C*). This suggested that the volume of fibrous tissues observed with MRI decreased in favor of an increasing volume of mineralized tissue. Moreover, the 3D reconstructions of the condyles' cartilage surface showed that the average cartilage area, measured based on 2 medial segments crossing the defect in its center (Figure 3, *D-E* for untreated control and BCT-implanted condyle, respectively) is almost three times as large in condyles transplanted with the BCT (Figure 3, *F*) than in those left untreated (Figure 3, *G*) (6.9 ± 3.6 $mm^2$ vs. 2.6 ± 1.8 $mm^2$, respectively; $p = 0.0030$; Figure 3, *H left chart*). These data were generated on all condyles considered, regardless to their anatomical locations; however, a similar picture (9.5 ± 4.1 $mm^2$ vs. 2.9 ± 0.8 $mm^2$, for BCT-treated and untreated defect condyles, respectively; $p = 0.0030$; Figure 3, *H right chart*) was observed when the same assessment was run on condyles of the left anterior limb only.

The aim of this study is to regenerate the whole osteochondral unit by using our combined ATMP. We further investigated the integration of the regeneration of both cartilage and subchondral bone after 6 months' transplantation. In Figure 4, we have shown the well regenerated junction between the newly regenerated cartilage and the subchondral bone (white dashed line in Figure 4, *A-C*).

In summary, the overall repair assessment based on both the ICRS scores, the quantitative analysis of the micro-CT scans and the histological analysis showed the effectiveness of the BCT in supporting the formation of a nearly normal cartilage and its integration with the surrounding tissue.

*Sulphated GAGs deposition and morphology of the chondrocytes as evidences of hyaline cartilage formation*

Current clinical therapeutics for cartilage repair have not sufficiently taken into account the importance of subchondral bone regeneration, which is essential for the mechanical functions of the joint and the maintenance of the overlying cartilage homeostasis. During microfracture procedures,

cartilage successfully regenerated, however compared to the native cartilage, it was limited in size and composed of fibrocartilage with lesser GAGs and increased vascularization than hyaline cartilage[41,42].

Histological evidences showing cartilage repair during human clinical trials are difficult to obtain, due to ethical considerations concerning the use of post-operative biopsies, which would unavoidably affect the repaired joint. The advantage of our sheep model was the possibility to evaluate *ex vivo* the histological quality of new osteochondral tissue formed during the 6 months following implantation (Figure 5). In general, the regenerated osteochondral unit in sheep implanted with the BCT (Figure 5, *B*) looked similar to that of wild type controls (Figure 5, *A*). Higher magnifications revealed that the superficial hydrogel part, dedicated to cartilage repair, fully adjusted with the fibrous part, devoted to subchondral bone regeneration. Also, the sustained presence of cells was observed in both compartments of the ATMP as well as in their junction, which is a paramount element to ensure tissue remodeling throughout the whole engineered osteochondral unit (Figure 5, *D*). On the other hand, the histological staining of the implant site with Alcian Blue allowed us to observe the abundant deposition of sulphated GAGs (circle in Figure 5, *C*), associated to areas where chondrocytes were more abundant (square in Figure 5, *C*). Interestingly, it appeared that a morphological gradient of the chondrocytes was observed, where an elongated shape was found closer to the articular surface (black arrowheads in Figure 5, *E-F*), while a rounded shape was found deeper, associated with the subchondral layer (green arrowheads in Figure 5, *E-F*). However, further studies have to conducted in order to rule out if such a gradient is found in all BCT-treated condyles and if it really depends on the improved BCT-driven regeneration. Altogether, these results indicate that our ATMP was able to efficiently induce the regeneration of the missing tissues within the induced defect that possess cytological (chondrocyte shape) and biochemical (deposition of GAGs) features that resemble those of the native hyaline cartilage.

## Discussion

Spontaneous wound healing of osteochondral defects remains very limited and may lead to secondary osteoarthritis over time. The well-established autologous chondrocytes implantation (ACI) approach is used in clinical practice. Nevertheless, chondrocytes need *in vitro* pre-amplification before implantation, responsible for the gradual phenotype loss. Chondrocyte dedifferentiation subsequently leads to fibrous cartilage formation, which does not satisfy the mechanical properties of native hyaline cartilage. To overcome the limitations associated with the restricted quantity of primary chondrocytes, mesenchymal stem cell-based therapies are expanding strategies for osteochondral repair[43–46], and have the ATMP status in several clinical trials[20]. In the cartilage repair field, the collected results are encouraging but still remain exploratory, and need confirmation in non-rodent animal models[47].

As clinical studies are not possible without supportive preclinical data collected from large animal studies, we focused on the application of autologous MSCs on critical defects in a sheep model. Indeed, we created critical lesions of 7 mm diameter by 3 mm depth to prevent their spontaneous repair. This type of procedure is clinically relevant, and cannot be realized in rodent animal models, due to the restricted dimensions of their joints and the fewer cell layers composing their articular cartilage[48]. Rodent animal studies generally obtain very encouraging results, however rarely replicable in human trials. On the other hand, ovine studies represent strategic animal models for knee cartilage regeneration as they display many comparable features to the human knee. Ovine models have a similar bicondylar femoral structure, with the meniscus and cruciate ligaments. Furthermore, they suffer similar mechanical stress than human knees, with similar sized joints, which is the most affected site by osteochondral lesions and secondary osteoarthritis[49,50].

New therapeutic strategies and biological approaches have made accessible innovative tools in order to support cartilage repair. These last years, third generation biomaterials, involving active molecules and living cells, seem to offer significant advantages in that objective[51–53]. Constructions with stratified materials, mimicking osteochondral features with layered interfaces, have the advantage to offer comparable mechanical characteristics mimicking the natural gradients of osteoarticular tissue[54,55]. The bi-compartmented therapeutics (BCT) evaluated in this pilot study offers the possibility to simultaneously promote the regeneration of subchondral bone and articular cartilage in an implantable device, easily useable for a one-step surgical procedure. The nanotechnology associated to this therapeutic approach offers a significant advantage for multi-tissue interfaced differentiation, as BMP-2 nanocontainers drive a local cell-contact dependent stimulation, when delivered in adequate dosage (nanoquantities).

It is noteworthy that restoring healthy subchondral bone is a key element participating to a stable long-lasting articular cartilage recovery after an occurrence of an osteochondral defect. Although the physiological crosstalk between bone and cartilage is incompletely understood, the mutual influence of these tissues on one another is supported by their anatomical proximity and common embryogenic background[56]. One of the most highlighted issues is related to the nutrients, oxygen and secreted factors from the subchondral bone to the overlying avascular cartilage[57]. Damaged subchondral bone compromises chondral repair through abnormal neoangiogenesis, jeopardizing the physiological hypoxic environment of cartilage. Microvascular invasion of injured chondral tissue, and therefore improper diffusion of pro-inflammatory factors[58], associated with an increased nutrient and oxygen supply, are the archstones of secondary osteoarthritis. Thus, subchondral bone appears to be a regulatory interface between cartilage and trabecular bone, rather than a simple mechanical support.

We previously investigated restoration of the subchondral plate by developing functionalized materials with osteogenic factors, like BMP-2 or BMP-7[16,17]. The functionalized wound dressing was able to

efficiently support single cells (MSCs) for bone and cartilage regeneration[25,26,31]. In order to regenerate effectively the joint cartilage, we associated BMP-2 functionalized collagen wound dressing with a superficial hydrogel made of alginate and hyaluronic acid mix solution. Alginate and hyaluronic acid are well known to enhance chondrogenic differentiation[19,28]. To mimic the cell condensation that initiates skeletogenesis[59], and optimize this specific lineage induction, hydrogel was amalgamated with autologous bone marrow MSCs organized as spheroids[29,36]. Our ATMP strategy using single cells (MSCs) had been validated in good laboratory practice (GLP) preclinical studies in rat and sheep models [31].

In order to avoid long term degeneration of the cartilage graft[60], we hypothesized that cartilage regeneration will be improved with a stable healthy subchondral environment, free from microvascular changes that are observed in osteoarthritis. Our histological results confirmed that the newly regenerated cartilage was hyaline-like. This could be explained by the innovative bi-compartmented structure of our implant, in which the nanofibrous layer may be able to prevent the vascular invasion of the superficial hydrogel.

In a human clinical trials, follow up of cartilage repair should be prolonged at least up to 2 years, and even 7 years after surgery[6,39]. In a 7 years follow-up clinical study, using an autologous matrix-induced chondrogenesis (AMIC) process (Chondro-Gide®), some authors showed that two thirds of the patients demonstrated great quality of chondral repair with no deterioration over time. With the same kind of procedure (AMIC), it was observed that clinical signs of repair became significantly visible only after 24 months post-implantation. However, deteriorations of tissue could also appear precociously after the surgical procedure (first months), showing that the implant behavior is unpredictable during the early post-implantation period. In our study, the implant was well integrated into the host tissue, because macroscopic aspect and MRI imaging revealed no delamination, nor displacement of a portion of the graft. We postulate that extracellular matrix deposition at the interface of the implant with the host tissue could explain the fusion of both neotissues, assuring sustainable integration of the neoformed osteochondral unit. Since the neoformed chondral tissue was histologically comparable to native hyaline cartilage, we hope that it will persist on the long term, with similar mechanical properties and an effective cross talk with the subchondral bone.

In conclusion, this study reveals the safety and efficiency of our nanoactive living implant, to simultaneously regenerate articular cartilage and subchondral bone, in an ovine model of critical knee defects. Our strategy is based on a hydrogel embedding of bone-marrow derived MSCs spheroids, recovering an underlying collagen membrane enriched with nanoreservoirs of BMP-2 growth factor. Our results established the feasibility and efficiency of this hybrid implant to support hyaline-like tissue formation, suggesting a promising impact on human osteochondral lesions repair. Therefore, this therapeutic strategy could be an adequate solution to effectively treat focal osteochondral defects,

in order to avoid progression to secondary osteoarthritis and prevent the burden of degenerative joint disease. Our technology is based on one step surgical procedure but necessitating previous MSC harvesting through bone marrow aspiration. This technology is adaptable and can use different kinds of therapeutics and stem cells including allogenic stem cells to avoid the bone marrow aspiration. This innovative approach should also find applications in other domains of complex tissue restoration.

**Author contributions**: N.B.-J. designed the research; H.F., L.P., J.S., L.K., and P.R. performed research; H.F., L.P., J.S., F.F., L.K., D.S., H.A., M.E., S.K.B., D.M., P.R., and N.B.-J. analyzed data; H.F., L.K., L.P., G.H., L.G., and N.B.-J. wrote the paper.

**Acknowledgments**: We would like to thank Natalia De Isla for help with cytometry protocol, Nadia Messaddeq and Julien Becker for micro-CT acquisitions, Jochen Barth for cytometry, for box plot acquisition and CIRE Platform for experimental surgery and imaging, Val de Loire INRA Centre, 37380 Nouzilly, France with Stéphanie Krissian for sheep surgery.

**References**


1. Hunter W. Of the structure and disease of articulating cartilages. 1743. Clin Orthop. 1995;**317**:3-6.

2. Logerstedt DS, Snyder-Mackler L, Ritter RC, Axe MJ, Orthopedic Section of the American Physical Therapy Association. Knee pain and mobility impairments: meniscal and articular cartilage lesions. J Orthop Sports Phys Ther. 2010;**40**(6):A1-35.

3. Pot MW, van Kuppevelt TH, Gonzales VK, Buma P, IntHout J, de Vries RBM, et al. Augmented cartilage regeneration by implantation of cellular versus acellular implants after bone marrow stimulation: a systematic review and meta-analysis of animal studies. PeerJ. 2017;**5**:e3927.

4. Mithoefer K, Saris DBF, Farr J, Kon E, Zaslav K, Cole BJ, et al. Guidelines for the Design and Conduct of Clinical Studies in Knee Articular Cartilage Repair: International Cartilage Repair Society Recommendations Based on Current Scientific Evidence and Standards of Clinical Care. Cartilage. 2011;**2**(2):100-21.

5. Volz M, Schaumburger J, Frick H, Grifka J, Anders S. A randomized controlled trial demonstrating sustained benefit of Autologous Matrix-Induced Chondrogenesis over microfracture at five years. Int Orthop. 2017;**41**(4):797-804.

6. Niethammer TR, Holzgruber M, Gülecyüz MF, Weber P, Pietschmann MF, Müller PE. Matrix based autologous chondrocyte implantation in children and adolescents: a match paired analysis in a follow-up over three years post-operation. Int Orthop. 2017;**41**(2):343-50.

7. Schuette HB, Kraeutler MJ, McCarty EC. Matrix-Assisted Autologous Chondrocyte Transplantation in the Knee: A Systematic Review of Mid- to Long-Term Clinical Outcomes. Orthop J Sports Med. 2017;**5**(6).

8. Hjelle K, Solheim E, Strand T, Muri R, Brittberg M. Articular cartilage defects in 1,000 knee arthroscopies. Arthrosc J Arthrosc Relat Surg Off Publ Arthrosc Assoc N Am Int Arthrosc Assoc. 2002;**18**(7):730-4.

9. Hench LL, Polak JM. Third-generation biomedical materials. Science. 2002;**295**(5557):1014-7.

10. Navarro M, Michiardi A, Castaño O, Planell JA. Biomaterials in orthopaedics. J R Soc Interface. 2008;**5**(27):1137-58.

11. McKay WF, Peckham SM, Badura JM. A comprehensive clinical review of recombinant human bone morphogenetic protein-2 (INFUSE® Bone Graft). Int Orthop. 2007;**31**(6):729-34.

12. Tannoury CA, An HS. Complications with the use of bone morphogenetic protein 2 (BMP-2) in spine surgery. Spine J Off J North Am Spine Soc. 2014;**14**(3):552-9.

13. Quinlan E, Thompson EM, Matsiko A, O'Brien FJ, López-Noriega A. Long-term controlled delivery of rhBMP-2 from collagen-hydroxyapatite scaffolds for superior bone tissue regeneration. J Control Release Off J Control Release Soc. 2015;**207**:112-9.

14. Zara JN, Siu RK, Zhang X, Shen J, Ngo R, Lee M, et al. High doses of bone morphogenetic protein 2 induce structurally abnormal bone and inflammation in vivo. Tissue Eng Part A. 2011;**17**(9-10):1389-99.

15. James AW, LaChaud G, Shen J, Asatrian G, Nguyen V, Zhang X, et al. A Review of the Clinical Side Effects of Bone Morphogenetic Protein-2. Tissue Eng Part B Rev. 2016;**22**(4):284-97.

16. Mendoza-Palomares C, Ferrand A, Facca S, Fioretti F, Ladam G, Kuchler-Bopp S, et al. Smart hybrid materials equipped by nanoreservoirs of therapeutics. ACS Nano. 2012;**6**(1):483-90.

17. Eap S, Ferrand A, Schiavi J, Keller L, Kokten T, Fioretti F, et al. Collagen implants equipped with 'fish scale'-like nanoreservoirs of growth factors for bone regeneration. Nanomed. 2014;**9**(8):1253-61.

18. Seo S, Na K. Mesenchymal stem cell-based tissue engineering for chondrogenesis. J Biomed Biotechnol. 2011;806891.

19. Beane OS, Darling EM. Isolation, characterization, and differentiation of stem cells for cartilage regeneration. Ann Biomed Eng. 2012;**40**(10):2079-97.

20. Slaper-Cortenbach ICM. Current Regulations for the Production of Multipotent Mesenchymal Stromal Cells for Clinical Application. Transfus Med Hemotherapy Off Organ Dtsch Ges Transfusionsmedizin Immunhamatologie. 2008;**35**(4):295-8.

21. Gómez-Barrena E, Solá CA, Bunu CP. Regulatory authorities and orthopaedic clinical trials on expanded mesenchymal stem cells. Int Orthop. 2014;**38**(9):1803-9.

22. Goldberg A, Mitchell K, Soans J, Kim L, Zaidi R. The use of mesenchymal stem cells for cartilage repair and regeneration: a systematic review. J Orthop Surg. 2017;12(1):39.

23. Zhang L, Su P, Xu C, Yang J, Yu W, Huang D. Chondrogenic differentiation of human mesenchymal stem cells: a comparison between micromass and pellet culture systems. Biotechnol Lett. 2010;**32**(9):1339-46.

24. Sasaki J-I, Matsumoto T, Egusa H, Matsusaki M, Nishiguchi A, Nakano T, et al. In vitro reproduction of endochondral ossification using a 3D mesenchymal stem cell construct. Integr Biol Quant Biosci Nano Macro. 2012;**4**(10):1207-14.

25. Eap S, Keller L, Schiavi J, Huck O, Jacomine L, Fioretti F, et al. A living thick nanofibrous implant bifunctionalized with active growth factor and stem cells for bone regeneration. Int J Nanomedicine. 2015;**10**:1061-75.

26. Schiavi J, Keller L, Morand D-N, De Isla N, Huck O, Lutz JC, et al. Active implant combining human stem cell microtissues and growth factors for bone-regenerative nanomedicine. Nanomed. 2015;**10**(5):753-63.

27. Leijten J, Teixeira LSM, Bolander J, Ji W, Vanspauwen B, Lammertyn J, et al. Bioinspired seeding of biomaterials using three dimensional microtissues induces chondrogenic stem cell differentiation and cartilage formation under growth factor free conditions. Sci Rep. 2016;**6**:36011.

28. Keller L, Wagner Q, Schwinté P, Benkirane-Jessel N. Double compartmented and hybrid implant outfitted with well-organized 3D stem cells for osteochondral regenerative nanomedicine. Nanomed. 2015;**10**(18):2833-45.

29. Keller L, Schwinté P, Gomez-Barrena E, Arruebo M, Benkirane-Jessel N. Smart Implants as a Novel Strategy to Regenerate Well-Founded Cartilage. Trends Biotechnol. 2017;**35**(1):8-11.

30. Keller L, Wagner Q, Pugliano M, Breda P, Ehlinger M, Schwinte P, et al. Bi-layered nano active implant with hybrid stem cell microtissues for tuned cartilage hypertrophy. J Stem Cell Res Ther. 2015;**1**(1).

31. Keller L, Pijnenburg L, Idoux-Gillet Y, Bornert F, Benameur L, Tabrizian M, et al. Preclinical safety study of a combined therapeutic bone wound dressing for osteoarticular regeneration. Nat Commun. 2019;**10**(1):2156.

32. Dominici M, Le Blanc K, Mueller I, Slaper-Cortenbach I, Marini F, Krause D, et al. Minimal criteria for defining multipotent mesenchymal stromal cells. The International Society for Cellular Therapy position statement. Cytotherapy. 2006;**8**(4):315-7.

33. Friedenstein AJ, Chailakhyan RK, Gerasimov UV. Bone marrow osteogenic stem cells: in vitro cultivation and transplantation in diffusion chambers. Cell Tissue Kinet. 1987;**20**(3):263-72.

34. McCarty RC, Gronthos S, Zannettino AC, Foster BK, Xian CJ. Characterisation and developmental potential of ovine bone marrow derived mesenchymal stem cells. J Cell Physiol. 2009;**219**(2):324-33.

35. Boxall SA, Jones E. Markers for characterization of bone marrow multipotential stromal cells. Stem Cells Int. 2012;975871.

36. Bécavin T, Kuchler-Bopp S, Kökten T, Huck O, Messaddeq N, Lesot H, et al. Well-organized spheroids as a new platform to examine cell interaction and behaviour during organ development. Cell Tissue Res. 2016;**366**(3):601-15.

37. Chang G, Sherman O, Madelin G, Recht M, Regatte R. MR imaging assessment of articular cartilage repair procedures. Magn Reson Imaging Clin N Am. 2011;**19**(2):323-37.

38. Guermazi A, Roemer FW, Alizai H, Winalski CS, Welsch G, Brittberg M, et al. State of the Art: MR Imaging after Knee Cartilage Repair Surgery. Radiology. 2015;**277**(1):23-43.

39. Alparslan L, Winalski CS, Boutin RD, Minas T. Postoperative magnetic resonance imaging of articular cartilage repair. Semin Musculoskelet Radiol. 2001;**5**(4):345-63.

40. Anderson DE, Williams RJ, DeBerardino TM, Taylor DC, Ma CB, Kane MS, et al. Magnetic Resonance Imaging Characterization and Clinical Outcomes After NeoCart Surgical Therapy as a Primary Reparative Treatment for Knee Cartilage Injuries. Am J Sports Med. 2017;**45**(4):875-83.

41. Erggelet C, Endres M, Neumann K, Morawietz L, Ringe J, Haberstroh K, et al. Formation of cartilage repair tissue in articular cartilage defects pretreated with microfracture and covered with cell-free polymer-based implants. J Orthop Res Off Publ Orthop Res Soc. 2009;**27**(10):1353-60.

42. Kang S-W, Bada LP, Kang C-S, Lee J-S, Kim C-H, Park J-H, et al. Articular cartilage regeneration with microfracture and hyaluronic acid. Biotechnol Lett. 2008;**30**(3):435-9.

43. Medvedeva EV, Grebenik EA, Gornostaeva SN, Telpuhov VI, Lychagin AV, Timashev PS, et al. Repair of Damaged Articular Cartilage: Current Approaches and Future Directions. Int J Mol Sci. 2018;**19**(8).

44. Patel DM, Shah J, Srivastava AS. Therapeutic potential of mesenchymal stem cells in regenerative medicine. Stem Cells Int. 2013;496218.

45. Picinich SC, Mishra PJ, Mishra PJ, Glod J, Banerjee D. The therapeutic potential of mesenchymal stem cells. Cell- & tissue-based therapy. Expert Opin Biol Ther. 2007;**7**(7):965-73.

46. Reible B, Schmidmaier G, Moghaddam A, Westhauser F. Insulin-Like Growth Factor-1 as a Possible Alternative to Bone Morphogenetic Protein-7 to Induce Osteogenic Differentiation of Human Mesenchymal Stem Cells in Vitro. Int J Mol Sci. 2018;**19**(6).

47. Lee WY-W, Wang B. Cartilage repair by mesenchymal stem cells: Clinical trial update and perspectives. J Orthop Transl. 2017;**9**:76-88.

48. Chu CR, Szczodry M, Bruno S. Animal models for cartilage regeneration and repair. Tissue Eng Part B Rev. 2010;**16**(1):105-15.

49. Ahern BJ, Parvizi J, Boston R, Schaer TP. Preclinical animal models in single site cartilage defect testing: a systematic review. Osteoarthritis Cartilage. 2009;**17**(6):705-13.

50. Moran CJ, Ramesh A, Brama PAJ, O'Byrne JM, O'Brien FJ, Levingstone TJ. The benefits and limitations of animal models for translational research in cartilage repair. J Exp Orthop. 2016;**3**(1):1.

51. Lin T-H, Wang H-C, Cheng W-H, Hsu H-C, Yeh M-L. Osteochondral Tissue Regeneration Using a Tyramine-Modified Bilayered PLGA Scaffold Combined with Articular Chondrocytes in a Porcine Model. Int J Mol Sci. 2019;**20**(2).

52. Matsiko A, Levingstone TJ, O'Brien FJ. Advanced Strategies for Articular Cartilage Defect Repair. Mater Basel Switz. 2013;**6**(2):637‑68.

53. O'Brien FJ. Biomaterials & scaffolds for tissue engineering. Mater Today. 2011;**14**(3):88‑95.

54. Castro NJ, Hacking SA, Zhang LG. Recent progress in interfacial tissue engineering approaches for osteochondral defects. Ann Biomed Eng. 2012;**40**(8):1628‑40.

55. Nooeaid P, Schulze-Tanzil G, Boccaccini AR. Stratified Scaffolds for Osteochondral Tissue Engineering. Methods Mol Biol Clifton NJ. 2015;**1340**:191‑200.

56. Sharma AR, Jagga S, Lee S-S, Nam J-S. Interplay between cartilage and subchondral bone contributing to pathogenesis of osteoarthritis. Int J Mol Sci. 2013;**14**(10):19805‑30.

57. Findlay DM. Vascular pathology and osteoarthritis. Rheumatol Oxf Engl. 2007;**46**(12):1763‑8.

58. Funck-Brentano T, Cohen-Solal M. Crosstalk between cartilage and bone: when bone cytokines matter. Cytokine Growth Factor Rev. 2011;**22**(2):91‑7.

59. Hall BK, Miyake T. All for one and one for all: condensations and the initiation of skeletal development. BioEssays News Rev Mol Cell Dev Biol. 2000;**22**(2):138‑47.

60. Boushell MK, Hung CT, Hunziker EB, Strauss EJ, Lu HH. Current strategies for integrative cartilage repair. Connect Tissue Res. 2017;**58**(5):393‑406.

Figure 1. Schematic view of the implant of the bi-compartmented therapeutics for osteochondral regeneration. Mesenchymal stem cells (MSCs) were isolated from iliac crest bone marrow of B5 sheep. After proper characterization, MSCs were cultured in hanging drops to form autologous MSC spheroids. Concomitantly, collagen membranes were functionalized with BMP-2 nano-containers, by sequential deposition. A critical size defect with a diameter of 7 mm and 3 mm of depth was created in the medial femoral condyle of the sheep. The nano-functionalized device was placed in the osteochondral lesions and covered by the MSC hydrogel. Eventually the hydrogel was cross linked with $CaCl_2$. The osteochondral regeneration was monitored via MRI for 6 months in the living sheep and post-mortem according to the ICRS scoring system.

Figure 2. Non-invasive monitoring of the treated sheep articulations via longitudinal magnetic resonance imaging (MRI). **(A-I)** Sagittal MRI acquisitions of wild-type condyle **(A-C),** and of condyles with induced osteochondral defect **(D-I)**, either left untreated **(D-F)** or implanted with the BCT **(G-I).** Imaging was performed immediately after the surgery **(A, D and G)** and after 3 **(B, E and H)** and 6 months **(C, F and I)** from surgery. Red dashed lines indicate the extension of edema-like, hyper-intense T2 weighted signals in subchondral sites, which is commonly found after osteochondral surgery; cyan dashed line indicate the extension of non-hyper-intense T2 weighted signal in the trabecular bone. **(J)** In order to quantify the area covered by the hyper-intense signal, images were subject to the reduction of the grey levels in ImageJ (same parameters applied to all images), followed by binary conversion. A region of Interest (ROI) was drawn (red dashed lines) for each specimen and its area normalized against the average ROI area of untreated control condyles at t0. The results of the quantification are displayed in a dot plot. **: $p \leq 0.05$; n = 6 for each experimental group.

Figure 3. Post-mortem analysis of the condyles. **(A-B)** Six months after surgery, medial femoral condyles where the osteochondral defects were induced were explanted. Condyles were macroscopically assessed according to the ICRS score system. For more clarification, we have added Outerbridge classification: * (IB) ** (IIIA). **(A)**. Individual scores were assigned to each joint in respect to the degree of defect repair, the integration to the border zone (BCT only) and the macroscopic appearance of the cartilage. Data are presented in hybrid violin/dot-plot charts **(B)**. Each dot represents the average score based on 3 independent counts (n = 6). Scale bar in A: 5 mm. *: $p \leq 0.1$. **(C-H)** Explanted joints were imaged via micro-CT. Medial slides (C, upper panels), as well as the 3D surface rendering of the condyles (C, mid and lower panels) are presented for 3 untreated control (Ctrl) and 3 transplanted (BCT) condyles. As reference, a wild-type condyle is also presented (wt). Scale bars: 2 mm. (**D**-**H**) The average cartilage area was measured based on 2 medial segments crossing the defect in its center (yellow arrows in D,E). Trans-sectional surfaces were measured on successive medial slides of acquisitions, in order to provide an estimation of the thickness of the regenerated cartilage in each specimen (F,G). Cartilage is displayed in grey (Ca), while subchondral (Sb) and trabecular (Tb) bones are displayed in white. All values from left anterior, left posterior, right

anterior and right posterior femoral condyles are shown (H, left chart; n = 10 for each group); values from the left anterior femoral condyles only are also shown (H, right chart; n = 4 for each group). **: $p \leq 0.05$; ***: $p \leq 0.005$. Scale bar in C, D-G: 2 mm.

Figure 4. Morphology of the subchondral bone and trabecular bone 6 months after the transplantation of the BCT. (**A-C**) Biopsies from the implant site were histologically analyzed 6 months after surgery. Tissue sections were stained with Safranin O-Fast Green. Ca: cartilage; Sb: subchondral bone; Tb: Trabecular bone. White dashed line: tidemark; * in A corresponds to zoom in B and ** in A corresponds to zoom in C. Scale bar in A: 1 mm; B and C: 100 µm.

Figure 5. Morphology of the osteochondral unit 6 months after the transplantation of the BCT. **(A-F)** Biopsies from the implant site were histologically analyzed 6 months after surgery. Tissue sections were stained with either Safranin O-Fast Green **(A,B)** or Alcian Blue **(C-F)**. In all micrographies, the articular surface is to the top. The morphology of the osteochondral unit in animals implanted with the BCT (B) is similar to that found in wild-type animals (A). Scale bar in A, B: 100 µm. Sulphated glycosaminoglycans (GAGs), stained in orange/red after Alcian Blue staining, were abundant in BCT-implanted sheep (circle in C), adjacent to areas with a higher chondrocyte density (square in C). hb: host bone; scale bar in C: 100 µm. A cellularized "junction zone" was observed (yellow dashed lines in D) between the hydrogel (cartilaginous; ** in D) compartment and the fibrous (subchondral bone; * in D) compartment. Scale bar in D: 50 µm. The morphology of the chondrocytes changed from elongated in the proximal region (black arrowheads in E, F) to round in the chondroplast (green arrowheads in E, F), exhibiting a morphological gradient within the newly formed articular cartilage. **: cartilaginous part of the implant; *: nano-fibrous part of the implant; scale bar in E: 50 µm; in F: 25 µm.

## Figure 1 - 1 column-fitting

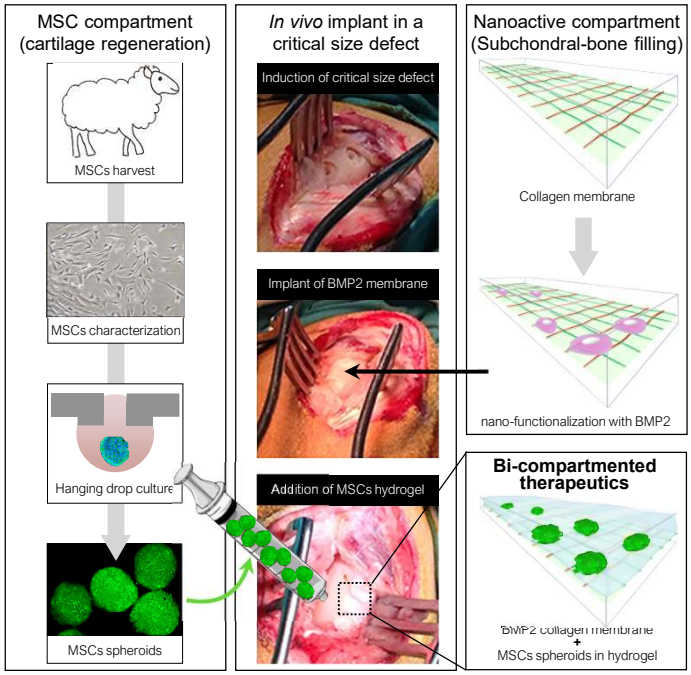

## Figure 2 - 1 column-fitting

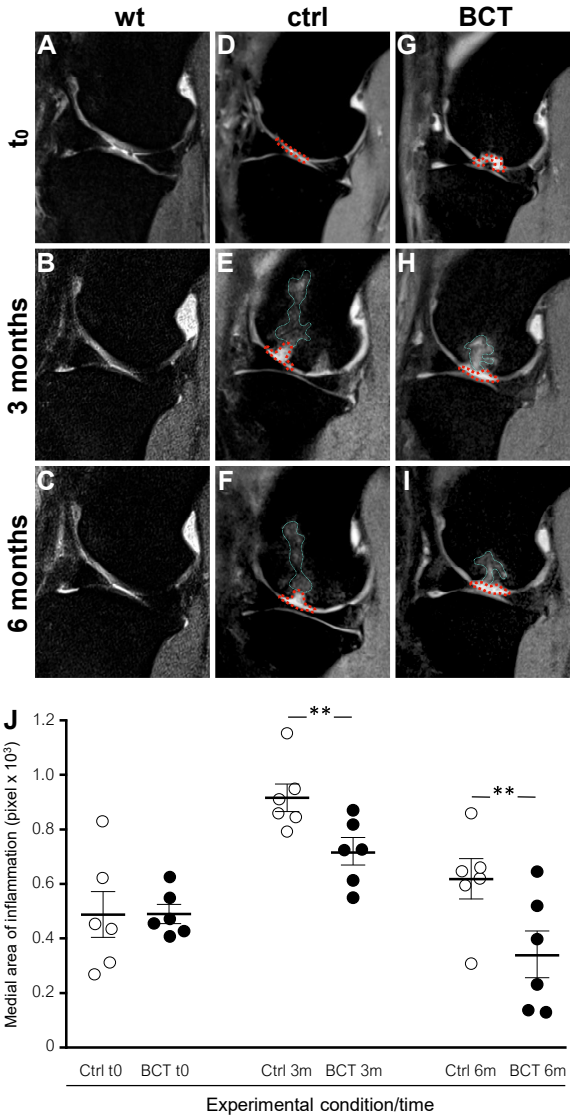

## Figure 3 - 2 columns

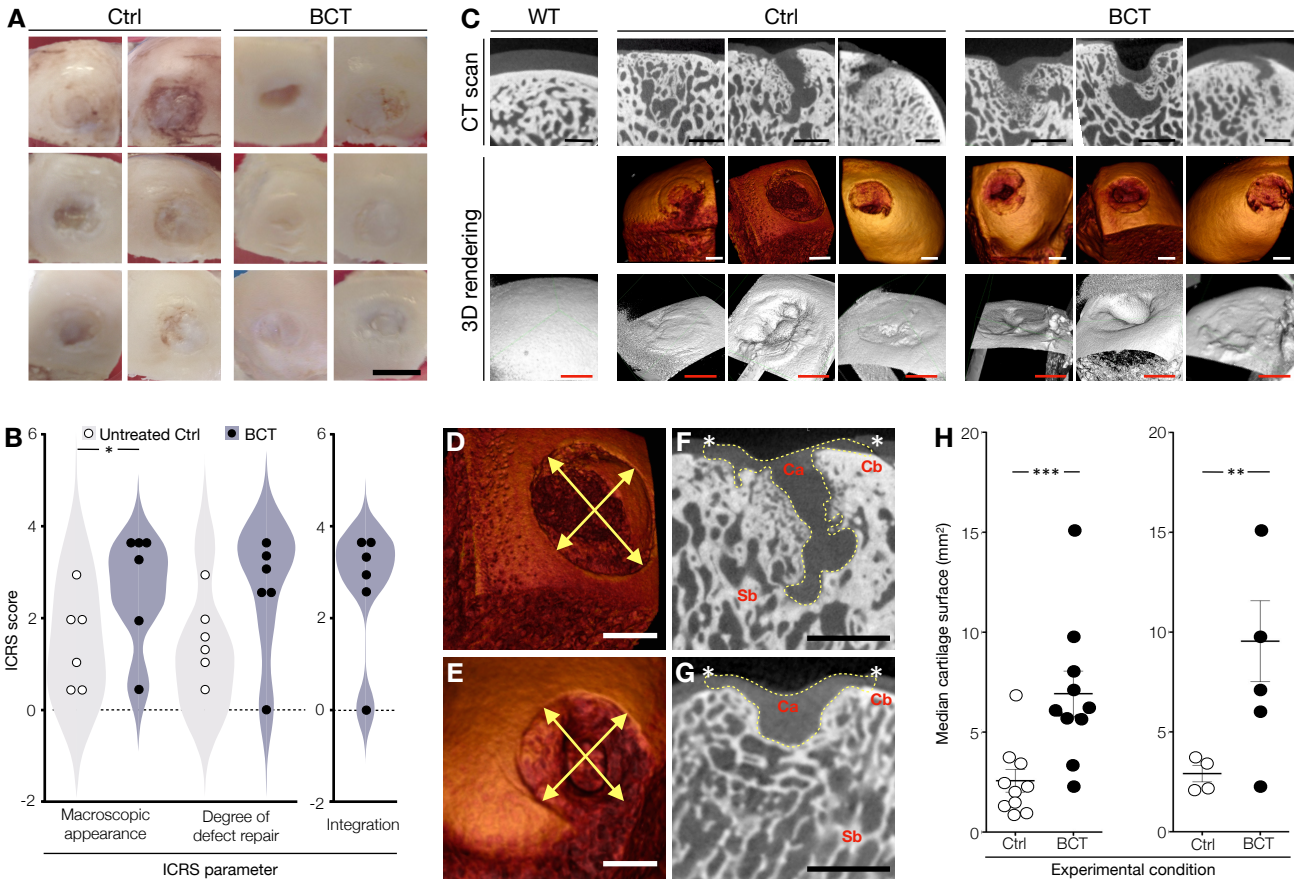

**Figure 4 - 1.5-column fitting**

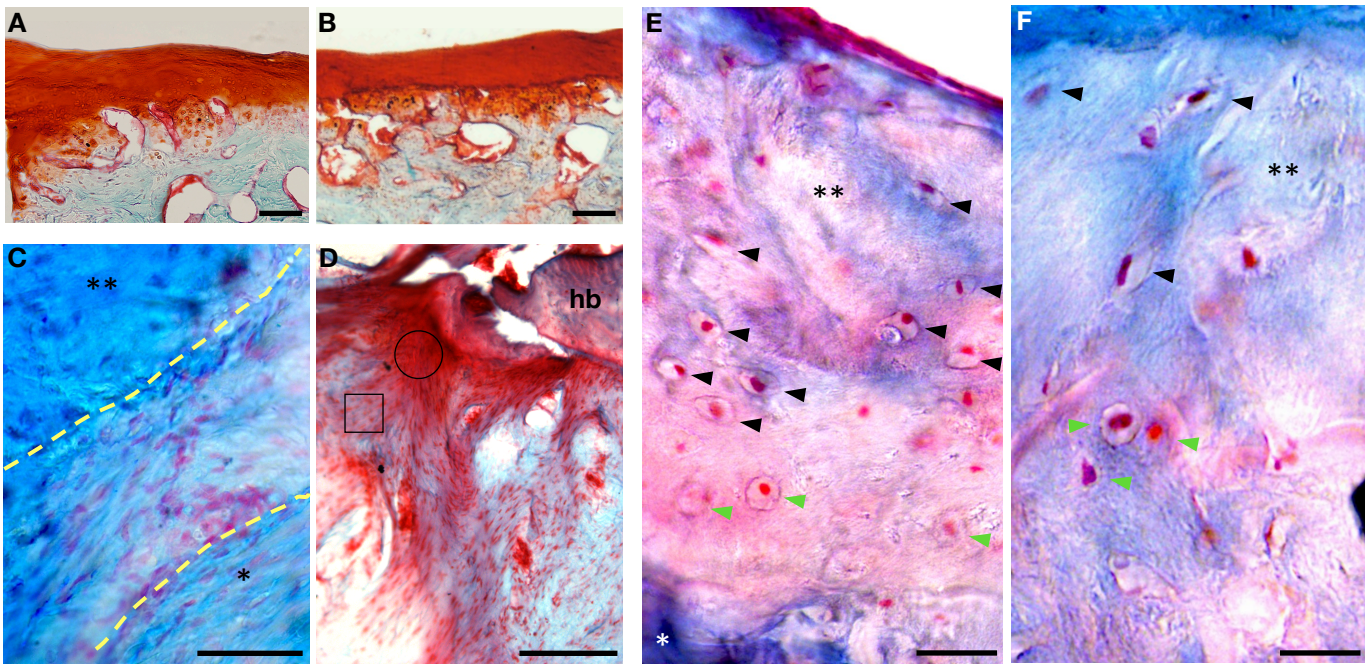

In this manuscript, we report the preclinical evaluation, in a big animal model, of a hybrid implant, composed of a living compartment based on stem cell spheroids and an underlying functionalized matrix with sustained release of therapeutics, as a candidate for treatments of articular cartilage lesions. Our technology approach fulfils the goals of regenerating more robust subchondral bone, in a shorter time frame. This would help to improve the therapeutic efficacy of the current, less sophisticated implants in the field of osteochondral regenerative surgery.

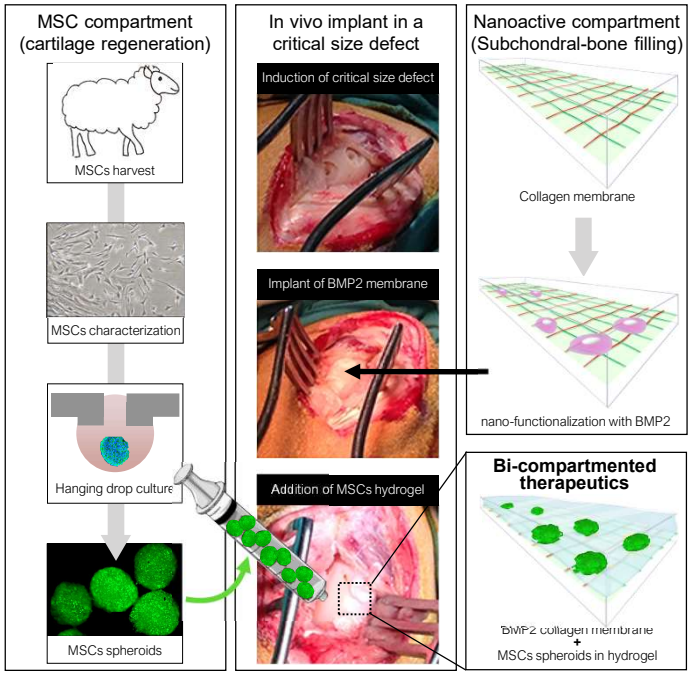
MSC compartment
(cartilage regeneration)
MSCs harvest
MSCs characterization
Hanging drop culture
MSCs spheroids
In vivo implant in a
critical size defect
Induction of critical size defect
Implant of BMP2 membrane
Addition of MSCs hydrogel
Nanoactive compartment
(Subchondral-bone filling)
Collagen membrane
nano-functionalization with BMP2
Bi-compartmented
therapeutics
BMP2 collagen membrane
+
MSCs spheroids in hydrogel